Soil Failure Mechanism for Lateral and Upward Pipeline–Soil Interaction Analysis in Dense Sand

Kshama Roy & Bipul Hawlader
Memorial University of Newfoundland, St. John's, NL, Canada
Shawn Kenny
Carleton University, Ottawa, ON, Canada

GEOQuébec 2015
Challenges from North to South
Des défis du Nord au Sud

ABSTRACT
Finite element (FE) simulation of the response of buried pipelines due to lateral and upward relative displacements is presented in this paper. Analyses are performed using the Arbitrary Lagrangian-Eulerian (ALE) approach available in Abaqus/Explicit FE software adopting a modified Mohr-Coulomb model (MMC) where pre-peak hardening, post-peak softening, density and confining pressure dependent friction and dilation angles are considered. The calculated peak dimensionless force with the MMC model is consistent with the available design guidelines for shallow burial depths. However, at deep burial conditions FE simulations with the Mohr-Coulomb (MC) model give higher peak resistance than the simulations with MMC model. The simulations with the MMC model appeared to be consistent with the trend of model test results. The role of strain-softening on soil resistance and failure pattern is also critically examined.

RÉSUMÉ
La simulation par éléments finis (EF) de la réponse de canalisations enfouies soumises à des déplacements relatifs latéraux et vers le haut est présentée dans cet article. Des analyses utilisant l'approche Lagrangienne-Eulérienne Arbitraire (LEA), disponible dans le logiciel d'EF Abaqus/Explicit, sont effectuées en utilisant un modèle Mohr-Coulomb modifié (MCM) considérant l'écrouissage pré-pic, le ramollissement post-pic, des angles de frottement et de dilatance dépendants de la densité et du confinement. La force sans dimension maximale calculée avec le modèle MCM est conforme aux lignes directrices de conception disponibles pour les profondeurs d'enfouissement peu profondes. Cependant, dans des conditions d'enfouissement profond, les simulations par EF utilisant le modèle Mohr-Coulomb (MC) donnent des résistances de pointe plus élevées que les simulations avec le modèle MCM. Les simulations utilisant le modèle MCM semblaient être conformes à la tendance observée pour des résultats de test par modèle. L'influence du ramollissement sur la résistance des sols et sur les modes de rupture est également examinée.

1 INTRODUCTION

With the increasing demand of energy, many major pipeline projects are being pursued by major oil and gas companies to diversify the business and also to add incremental values to existing assets. Key areas of focus for these projects include design of pipelines for transporting large quantities of crude oil over large distances. According to the Canadian Energy Pipeline Association (CEPA), in Canada, a network of approximately 115,000 km of underground energy transmission pipelines operates every day transporting oil and natural gas (http://www.cepa.com/). One of the major concerns for designing pipelines is to ensure very minimum risks to public and the environments. Geohazards and the associated ground movements represent a significant threat to pipeline integrity that may result in pipeline damage and failure (O'Rourke and Liu, 2012). In certain situations, pipelines might pass through a zone of potential ground failures, such as surface faulting, liquefaction-induced soil movements, and landslide induced permanent ground deformation (PGD). These ground movements might cause excessive stresses in pipeline resulting in severe damage.

Several experimental, theoretical and numerical studies have been conducted in the past to estimate the forces acting on pipelines due to relative movement of the soil in specific directions, namely axial, lateral and upward (e.g. Audibert and Nyman, 1978; Dickin and Leung, 1983; Trautmann, 1983; Paulin, 1998; White et al., 2001; Yimsiri et al., 2004; Guo and Stolle, 2005; Chin et al., 2006; Schupp et al., 2006; Byrne et al., 2008; Cheuk et al., 2008; Wijewickreme et al., 2009; Wang et al., 2010; Daiyan et al., 2011; Jung et al., 2013a&b; Williams et al., 2013). Several pipeline design guidelines have been developed on the basis of these extensive research works, (e.g. ALA, 2001; PRCI, 2004; DNV, 2007). Most of the design guidelines focused on the peak force exerted on the pipe. But not only are the peak force, the shape of the force-displacement curves are also significantly influenced by several factors during pipeline-soil interaction.

Continuum finite element (FE) analyses have been performed in the past to simulate lateral and uplift pipeline-soil interaction in sand (e.g. Yimsiri et al., 2004; Jung et al., 2013). The influence of constitutive model of soil on pipeline response has also been examined in some studies (Yimsiri et al., 2004). In the existing guidelines, the resistance of soil against the movement of pipes is quantified using a friction angle of sand. But pre-peak hardening, post-peak softening, density and confining pressure dependent angle of internal friction and dilation angle are the common features observed in laboratory tests on dense sand. The mode of shearing, such as triaxial (TX) or plane strain (PS), also significantly influences the behaviour (Bolton, 1986). All these features of the stress–strain behaviour of dense sand have not been considered in the available guidelines or FE modeling.

The main objective of the present study is to simulate lateral and upward pipeline–soil interaction using Arbitrary Lagrangian-Eulerian (ALE) approach available in Abaqus/Explicit FE software implementing a modified Mohr-Coulomb (MMC) model for dense sand. FE simulations are compared with experimental and numerical test results available in the literature. Finally, failure mechanisms for both lateral and uplift pipeline–soil interaction for shallow to deep burial conditions are discussed.

2 FINITE ELEMENT FORMULATION

Two-dimensional pipeline–soil interaction analyses are conducted using the Abaqus/Explicit FE software. Typical FE mesh for a 300 mm outer diameter (*D*) pipe subjected to lateral and upward movement is shown in Figs. 1 and 2, respectively. Taking the advantage of symmetry, only half of the domain is modeled for upward loading (Fig. 2). A 4-node bilinear plane strain quadrilateral element (CPE4R) is used for FE modeling of soil. The pipe is modeled as a rigid body. The structured mesh (Figs. 1&2) is generated by Abaqus/cae by zoning the soil domain. Denser mesh is used near the pipe.

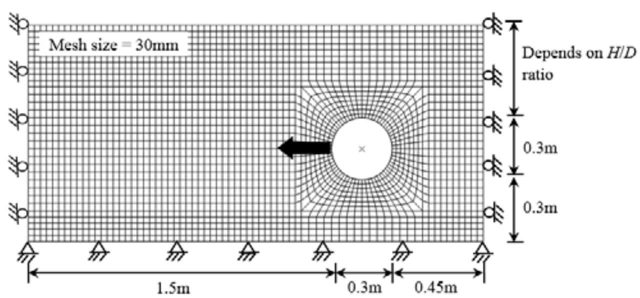

Figure 1. Typical finite element mesh for lateral loading for *D*=300mm and *H*/*D*=2

The bottom of the FE domain is restrained from horizontal and vertical movement, while all the vertical faces are restrained from any lateral movement using roller supports. No displacement boundary condition is applied on the top face and therefore soil can move freely. The centre of the pipe is placed at a distance *H* from the ground surface. The depth of the pipe is measured in terms of *H*/*D* ratio. The thickness of soil above the center of the pipe varies with *H*/*D* ratio. The locations of the bottom and left/right boundaries with respect to the location of the pipe are sufficiently large and therefore boundary effects on predicted lateral and uplift resistance, and soil failure mechanisms are not found.

The interface between pipe and soil is simulated using the contact surface approach available in Abaqus/Explicit. The Coulomb friction model is used for the frictional interface between the outer surface of the pipe and sand. In this method, the friction coefficient (μ) is defined as $\mu=\tan(\phi_\mu)$, where ϕ_μ is the pipe–soil interface friction angle. The value of ϕ_μ depends on the interface characteristics and relative movement between the pipe and soil. The value of μ equal to 0.32 is used in this study.

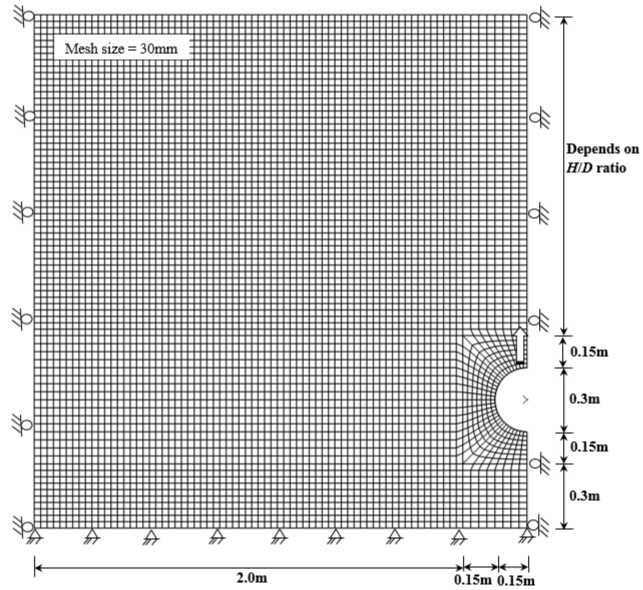

Figure 2. Typical finite element mesh for upward loading for *D*=300mm and *H*/*D*=6

The numerical analysis is conducted in two steps. In the first step, geostatic stress is applied while in the second step, the pipe is displaced in the lateral and upward direction specifying a displacement boundary condition at the reference point of the pipe.

3 MODELING OF SOIL

The Mohr-Coulomb (MC) model in its original form or after some modification has been used by many researchers in the past for pipeline–soil interaction analysis (e.g. Guo and Stolle, 2005; Xie, 2008; Daiyan et al., 2011; Kouretzis et al., 2013). In the present study, analyses are performed using the Mohr-Coulomb model in its original form (MC) and also after some modifications (MMC). In the Mohr-Coulomb model, for a given soil, constant values of angle of internal friction (ϕ') and dilation (ψ) are defined. However, the Modified Mohr-Coulomb Model (MMC) takes into account the effects of pre-peak hardening, post-peak softening, density and confining pressure on angles of internal friction (ϕ') and dilation (ψ) of dense sand. A detailed discussion of the MMC model and estimation of model parameters are available in Roy et al. (2014a&b) and is not repeated here. However, the constitutive equations are summarized in Table 1. The geometry and soil parameters used in the present FE analysis are shown in Table 2.

Abaqus does not have any direct option for modeling stress–strain behavior of the proposed MMC model; therefore, it is implemented using a user subroutine VUSDFLD. The plastic strain increment ($\Delta\gamma^p$) in each time increment is calculated as ($\Delta\gamma^p = \Delta\varepsilon^p_1 - \Delta\varepsilon^p_3$), where $\Delta\varepsilon^p_1$ and $\Delta\varepsilon^p_3$ are the major and minor principal plastic strain

Table 1: Equations for Modified Mohr-Coulomb Model (MMC) (summarized from Roy et al., 2014a&b)

Description	Eq. #	Constitutive Equation	Soil Parameters
Relative density index	(1)	$I_R = I_D(Q - \ln p') - R$	$I_D = D_r(\%)/100$, Q=10, R=1 (Bolton, 1986)
Peak friction angle	(2)	$\phi'_p - \phi'_c = A_\psi I_R$	ϕ'_c, A_ψ
Peak dilation angle	(3)	$\psi_p = \dfrac{\phi'_p - \phi'_c}{k_\psi}$	k_ψ
Strain softening parameter	(4)	$\gamma_c^p = C_1 - C_2 I_D$	C_1, C_2
Plastic strain at ϕ'_p	(5)	$\gamma_p^p = \gamma_c^p \left(p'/p'_a\right)^m$	p'_a, m
Mobilized friction angle at Zone-II	(6)	$\phi' = \phi'_{in} + \sin^{-1}\left[\left(\dfrac{2\sqrt{\gamma^p \gamma_p^p}}{\gamma^p + \gamma_p^p}\right)\sin\left(\phi'_p - \phi'_{in}\right)\right]$	
Mobilized dilation angle at Zone-II	(7)	$\psi = \sin^{-1}\left[\left(\dfrac{2\sqrt{\gamma^p \gamma_p^p}}{\gamma^p + \gamma_p^p}\right)\sin\left(\psi_p\right)\right]$	
Mobilized friction angle at Zone-III	(8)	$\phi' = \phi'_c + \left(\phi'_p - \phi'_c\right)\exp\left[-\left(\dfrac{\gamma^p - \gamma_p^p}{\gamma_c^p}\right)^2\right]$	
Mobilized dilation angle at Zone-III	(9)	$\psi = \psi_p \exp\left[-\left(\dfrac{\gamma^p - \gamma_p^p}{\gamma_c^p}\right)^2\right]$	
Young's modulus	(10)	$E = K p'_a \left(\dfrac{p'}{p'_a}\right)^n$	K, n

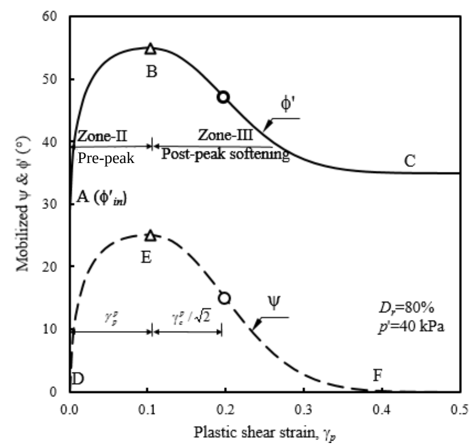

ϕ'_{in} = Initial peak friction angle, γ^p = Accumulated engineering plastic shear strain

components, respectively. The value of γ^p is calculated as the sum of $\Delta\gamma^p$ over the period of analysis. In the subroutine, γ^p and p' are defined as two field variables FV1 and FV2, respectively. In the input file, using Eqs. (1-9) (Table 1), the mobilized ϕ' and ψ are defined in tabular form as a function of γ^p and p'. During the analysis, the program accesses to the subroutine and updates the values of ϕ' and ψ with field variables.

4 RESULTS

4.1 Validation of FE model

The dashed lines in Figs. 3 and 4 show some experimental test results for the lateral and upward loading, respectively (Trautmann, 1983). The force–displacement curves are presented in normalized form, dimensionless lateral force N_h (=$F/\gamma HD$) with dimensionless lateral displacement u/D (Fig. 3) and dimensionless uplift force N_v (=$F/\gamma HD$) with dimensionless uplift displacement v/D (Fig. 4). Here F is the lateral/uplift force on the pipe per metre length, H is the depth of the centre of the pipe, γ is the unit weight of sand, u and v are the lateral and upward displacements respectively. The peak value of N_h and N_v are defined as N_{hp} and N_{vp}, respectively.

As shown, in both lateral (Fig. 3) and vertical (Fig. 4) loading, the dimensionless force increases with dimensionless displacement to the peak and then decreases. The post-peak decrease of the normalized force is high in the vertical loading as compared to the lateral loading. In order to show the performance of the MMC model, 4 analyses (2 lateral and 2 uplift) are performed and the results are compared with experimental test results (solid lines in Figs. 3 and 4). To be consistent with experimental tests, D=102 mm is used

Table 2**:** Parameters used in FE analyses

<table>
<tr><th rowspan="2">Parameters</th><th rowspan="2"></th><th colspan="2">Values</th></tr>
<tr><th>MC</th><th>MMC</th></tr>
<tr><td>Outer diameter of pipe, D (mm)</td><td></td><td colspan="2">300</td></tr>
<tr><td rowspan="3">Parameters for Young's modulus</td><td>K</td><td colspan="2">150</td></tr>
<tr><td>n</td><td colspan="2">0.5</td></tr>
<tr><td>p'_a (kN/m^2)</td><td colspan="2">100</td></tr>
<tr><td>Poisson's ratio, ν_{soil}</td><td></td><td colspan="2">0.2</td></tr>
<tr><td rowspan="6">Parameters for variation of $\phi'$and ψ</td><td>A_ψ</td><td>-</td><td>5</td></tr>
<tr><td>k_ψ</td><td>-</td><td>0.8</td></tr>
<tr><td>ϕ'_{in}</td><td>-</td><td>29°</td></tr>
<tr><td>C_1</td><td>-</td><td>0.22</td></tr>
<tr><td>C_2</td><td>-</td><td>0.11</td></tr>
<tr><td>m</td><td>-</td><td>0.25</td></tr>
<tr><td>Critical state friction angle, ϕ'_c</td><td></td><td>-</td><td>35°</td></tr>
<tr><td>Relative density, D_r (%)</td><td></td><td colspan="2">80</td></tr>
<tr><td>Unit weight, γ (kN/m^3)</td><td></td><td colspan="2">17.7</td></tr>
<tr><td>Interface friction coefficient, μ</td><td></td><td colspan="2">0.32</td></tr>
<tr><td>Depth of pipe, H/D</td><td></td><td colspan="2">Lateral (2, 4, 10, 15)
Uplift (2, 6, 15)</td></tr>
<tr><td>Friction angle for MC model</td><td></td><td>44°</td><td>-</td></tr>
<tr><td>Dilation angle for MC model</td><td></td><td>16°</td><td>-</td></tr>
</table>

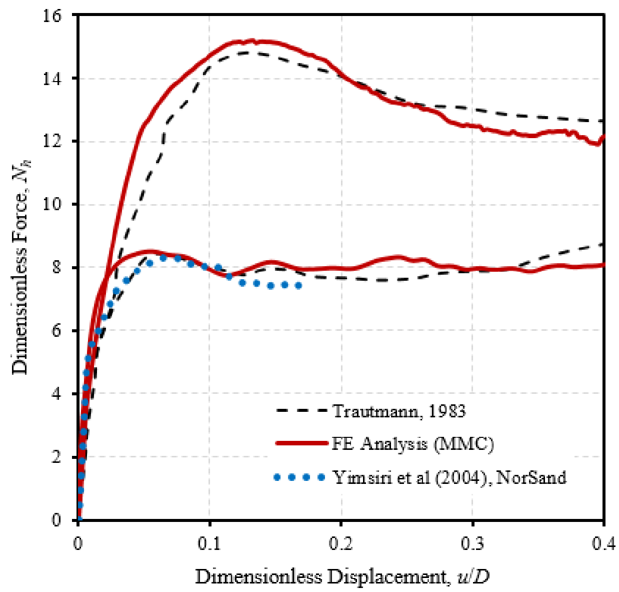

Figure 3. Force-displacement curves for lateral pipe loading tests for D=102mm, redrawn from Trautmann, 1983

in these sets of analyses. The force–displacement curves obtained from the FE analysis with the MMC model match very well for both lateral and upward pipe loading tests. Further details could be found in authors' previous studies (Roy et al., 2014a&b).Two FE analysis results with a complex NorSand soil constitutive model conducted by Yimsiri et al. (2004) are also plotted in Figs. 3 and 4. As shown, the simple MMC model can simulate the force–displacement curves including the post-peak degradation segments.

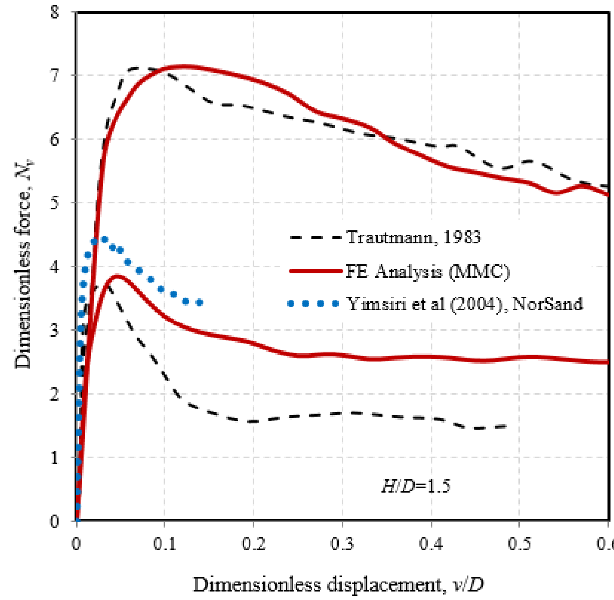

Figure 4. Force-displacement curves for uplift pipe loading tests for D=102mm, redrawn from Trautmann, 1983

4.2 Force–Displacement Behavior

Figure 5 shows the variation of dimensionless lateral force, N_h with dimensionless lateral displacement (u/D) for

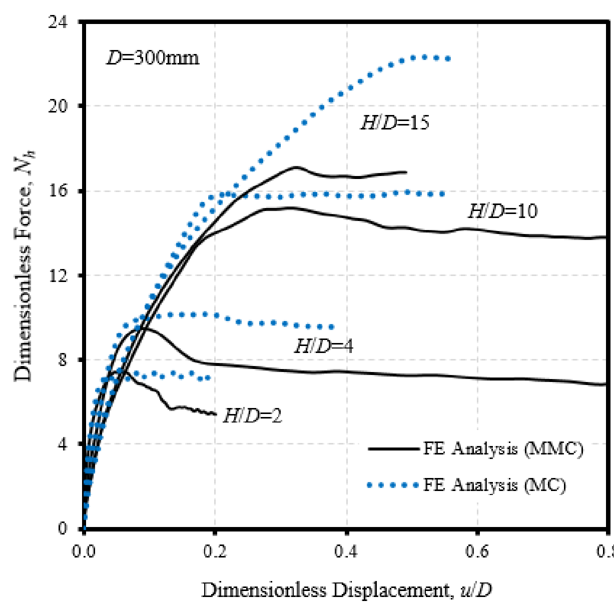

Figure 5. Comparison between MC and MMC for Lateral loading (D=300 mm)

different burial conditions obtained from FE analysis with the MC and MMC models. For shallow burial depths (*H*/*D*=2&4), the force–displacement curves with the MMC model show a strain-softening behavior after the peak, while the force–displacement curves with the MC model remains almost horizontal after the peak. This is due to the fact that in the MC model both ϕ' and ψ are constant. As shown in Fig. 3, post-peak degradation of normalized force was observed in the model test (Trautmann, 1983). For shallow to moderate burial depths (*H*/*D*=2, 4 & 10), the peak N_{hp} with the MMC model is comparable to the peak N_{hp} with the MC model when ϕ'=44° and ψ=16° is used. However, N_h with the MMC model at relatively large displacements after the peak is not comparable to the N_h with the MC model. This is due to the fact that the mobilized ϕ' and ψ approaches to the critical state in the MMC model, whereas in the MC both ϕ' and ψ remain constant even at large displacement. For a deep burial condition (*H*/*D*=15), the peak N_{hp} with the MC model is significantly higher than the N_{hp} with the MMC model. As the MMC model considers the pressure and plastic strain dependent ϕ' and ψ, the peak N_{hp} with the MMC model is lower than the N_{hp} with the MC model. The mean effective stress around the pipe is much higher in deep burial conditions than that in shallow burial condition and hence the peak friction angle is smaller which results lower peak N_{hp}.

Figure 6 shows the force–displacement curves for upward loading. For shallow to moderate burial depths, with the MMC model, N_v increases with vertical

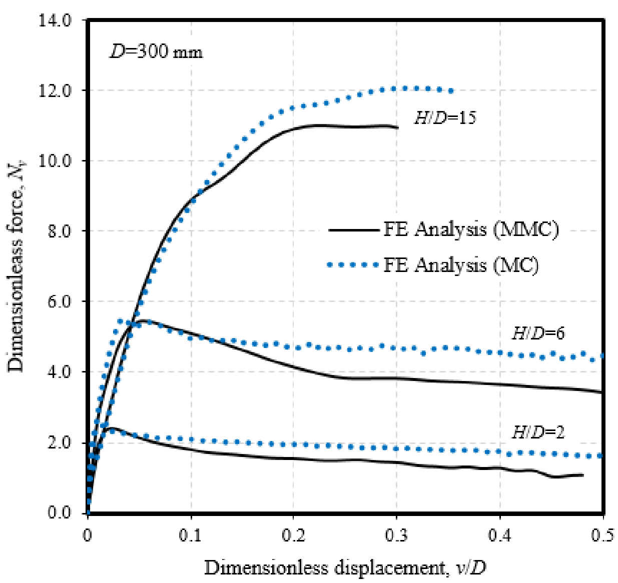

Figure 6. Comparison between MC and MMC for Uplift loading (*D*=300 mm)

displacement, reaches the peak and then decreases. Similar response (post-peak degradation of normalized force) was observed in the model tests conducted by Trautmann, 1983 (Fig. 4). For the MC model, there is a slight decrease in uplift force after the peak as the burial depth reduces with upward movement of the pipe. For deep burial conditions, the peak uplift force, N_{vp} with the MMC model is lower than the N_{vp} with MC model. This is due to the fact that in the MMC model, both ϕ' and ψ varies with plastic strain and p' whereas, MC model considers only constant ϕ' and ψ values. Therefore, the post-peak stress–strain behaviour of soil needs to be incorporated in the FE analysis for better simulation.

4.3 Peak Dimensionless Force versus Pipe Burial depth

The peak dimensionless force obtained from the present FE analyses for *D*=102 mm and 300 mm are plotted with *H*/*D* ratio in Figs. 7 and 8 for lateral and uplift loadings, respectively. For comparison, the results of experimental tests (Trautmann, 1983) and some design charts (Trautmann and O'Rourke, 1983, Yimsiri et al., 2004 and

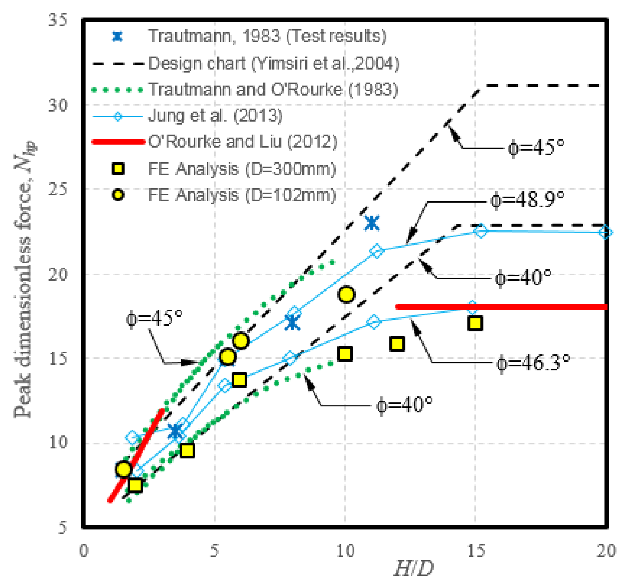

Figure 7. Dimensionless force vs *H*/*D* plot (Lateral)

Jung et al., 2013) available in the literature are also plotted on these figures. In Fig. 7, the N_{hp} increases with *H*/*D*. Although the curves are plotted as dimensionless force versus dimensionless displacement, they are not straight lines. This is due to the fact that different mechanisms control the behavior for different *H*/*D* ratios. The peak dimensionless forces from the present FE analyses at low *H*/*D* match well with the available design charts. But at higher *H*/*D* ratio, the peak N_{hp} obtained from the present FE analysis is much lower than the values calculated using existing guidelines. The trend of model tests (Trautmann and O'Rourke, 1983) appeared similar to the FE simulation with the MMC model. Jung et al. (2013) also used post-peak softening using a linear variation of angles of ϕ' and ψ with plastic strain, but did not consider the pre-peak hardening in their FE analyses and found smaller values of N_{hp} than Yimsiri et al. (2004) at higher *H*/*D* ratio. O'Rourke and Liu (2012) mentioned that for deep burial condition (*H*/*D*>12), the peak lateral force, N_{hp} becomes constant (solid line in Fig. 7) and this value can be calculated using a simple empirical equation

(N_{hp}=4μ+(1+K_p)(1+μ)-1.12(1+K_a)(0.44-0.89μ), where μ=tanϕ′, K_a and K_p are the Rankine active and passive earth pressure co-efficient, respectively. Their recommended value of N_{hp} is also smaller than that

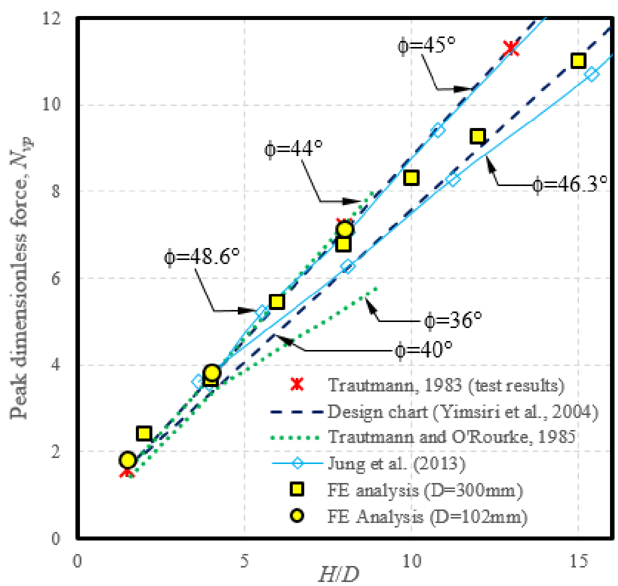

Figure 8. Dimensionless force vs H/D plot (Uplift)

predicted by the design charts. As discussed before, p' around the pipe increases with depth of burial, and that reduces the mobilized ϕ′ and ψ which in turn results in lower N_{hp}. If ϕ′ and ψ are independent of p', higher values of N_{hp} could be obtained especially for larger H/D as shown in Fig. 5 for the MC model (H/D=15). In the ALA guidelines, the shape of the N_{hp} versus H/D curves are similar to the Trautmann and O'Rourke (1983) but the values are significantly higher than the value obtained from the present FE analysis with the MMC model. Overestimation of N_{hp} has been also recognized in previous studies (Yimsiri et al., 2004; O'Rourke and Liu, 2012).

The calculated values of N_{vp} with the MMC model are plotted with H/D ratio in Fig. 8. Experimental results (Trautmann, 1983) and some design charts (Trautmann and O'Rourke, 1983, Yimsiri et al., 2004 and Jung et al., 2013) available in the literature are also plotted in this figure for further comparison. The N_{vp} increases almost linearly with H/D. The peak dimensionless force obtained from FE analyses compares very well with experimental results and design charts, even with constant values of ϕ′. The effect of pipe diameter is negligible compared to lateral loading as p' around the pipe for uplift loading is lower than that of lateral loading for same H/D ratio and same displacement. The peak N_{vp} becomes constant at very large H/D ratios as mentioned by Yimsiri et al. (2004) and Jung et al. (2013); however, in this study, simulations for very large depths are not performed. Although the peak force matches well for both MC and MMC, the failure patterns are different for both cases. For MC model a complete failure plane is developed at a displacement near the peak, and with further displacement, the dimensionless force does not change because ϕ' and ψ on this plane are constant. On the other hand, in MMC model, plastic strains mainly concentrate near the pipe when the peak dimensionless force is mobilized. With further displacement of the pipe, the size of the plastic zone increases and at a large displacement a complete failure plane develops. Details of the comparison in the failure mechanisms of MC and MMC models can be found in Roy et al. (2015).

5 SOIL FAILURE MECHANISM

5.1 Lateral Pipeline-Soil Interaction

Figure 9b shows the instantaneous velocity vectors for lateral loading at peak N_{hp} condition (u/D=0.05) for a shallow burial depth (H/D=2 and D=300mm). A simplified failure mechanism proposed by O'Rourke and Liu (2012) is also included Fig 9a. The failure mechanism at peak condition matches well with the O'Rourke and Liu (2012). Although it is not presented here, with increase in displacement, three distinct shear bands are formed which gradually reach the ground surface. Details of the shear band propagation pattern (failure mechanism) can be found at Roy et al. (2015).

The soil failure mechanisms for deep burial condition (H/D=15) are different from failure pattern for H/D=2. For H/D=15, a complete below ground zone of soil flow is observed. The plastic shear strain concentration mainly occurs near the pipe instead of reaching the ground surface. O'Rourke and Liu (2012) proposed a simplified four sided rigid block (abcde) failure mechanism for deep burial in sand as shown in Fig. 10a. Instantaneous velocity vectors from the present FE analysis at the peak N_{hp} condition (u/D=0.2) for deep burial depth (H/D=15 and D=300mm) is also plotted in Fig. 10b. As the pipe moves, the void left by the movement of the pipe is filled by soil following around the block. Fig 10 shows that the simplified failure wedge proposed by O'Rourke and Liu (2012) reasonably matches with the failure wedge from FE analysis with MMC. However, for deep burial condition, a number of shear bands form with increase in lateral displacement. Further studies are required for the failure mechanism at deep burial condition as very limited no of test results are available at deep burial condition.

5.2 Upward Pipeline-Soil Interaction

Figure 11a shows the displacement contours at u/D=0.2 for shallow burial depth (H/D=2). A similar failure mechanism for shallow burial condition was found by Ilamparuthi and Muthukrishnaiah (1999) for anchors buried in dense sand (Fig. 11b). For shallow burial depth at the peak resistance, the strain localization is occurred in a small zone of soil near the pipe. With increase in upward displacement, the extent of strain localization increases, and at a relatively large displacement, the shear band reaches the ground surface. Details of the failure pattern developed with MMC model can be found at Roy et al. (2015) and is not repeated here.

For deep burial condition (H/D=15), the failure mechanism is quite different. Figure 12a shows the

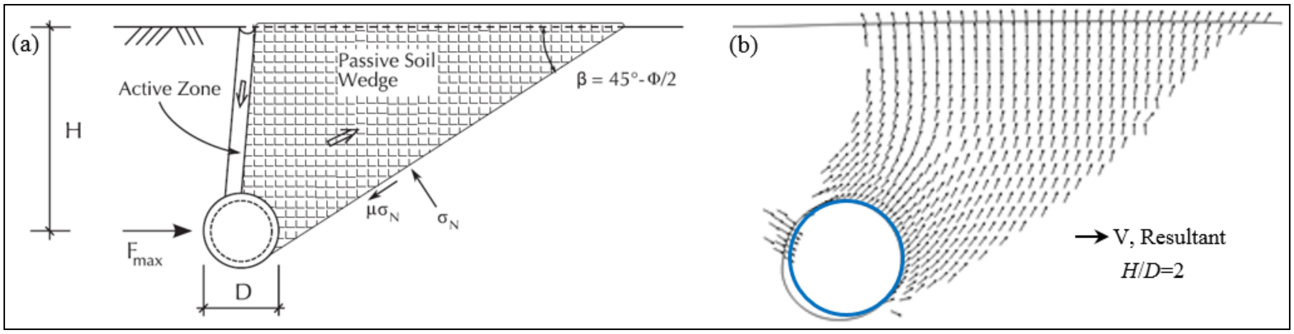

Figure 9. Comparison of failure wedge formation at shallow burial condition with (a) analytical model (O'Rourke and Liu, 2012) and (b) present FE analysis (instantaneous velocity vectors)

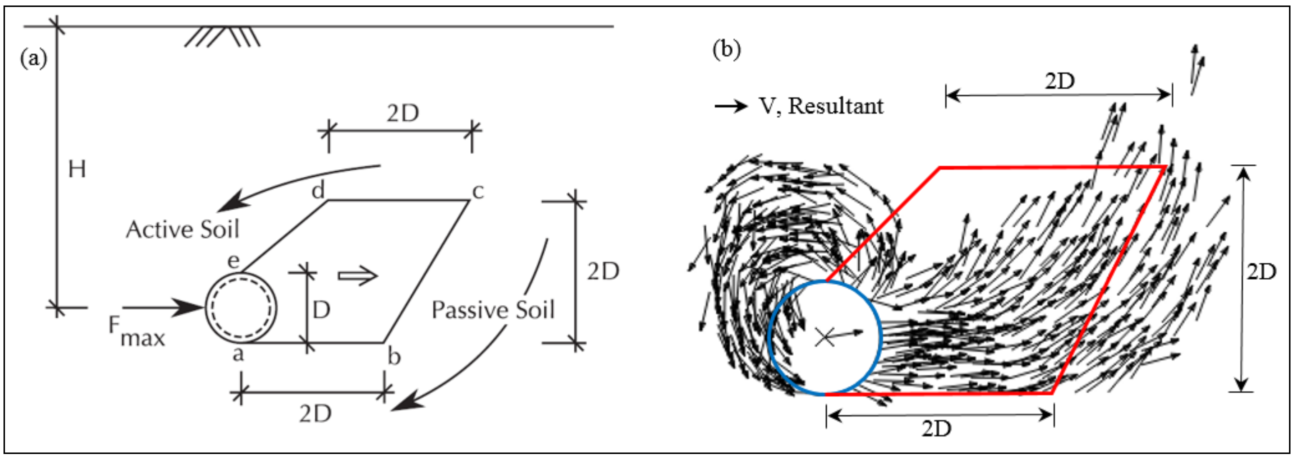

Figure 10. Comparison of failure wedge formation at deep burial condition with (a) analytical model (O'Rourke and Liu, 2012) and (b) present FE analysis (instantaneous velocity vectors)

displacement contours at *u*/*D*=0.2 for deep burial condition (*H*/*D*=15). The soil movement always remain below the ground surface (Fig 12a). The plastic shear strain concentration mainly occurs near the pipe. Similar failure mechanism for deep burial condition was found by Ilamparuthi and Muthukrishnaiah (1999) for anchors buried in dense sand (Fig. 12b).

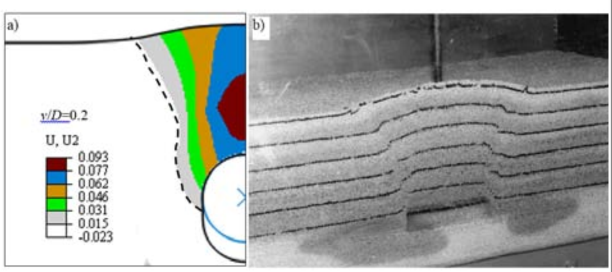

Figure 11. Soil failure mechanism for shallow burial condition: (a) Present FE analysis results (b) Test results for anchor, Ilamparuthi and Muthukrishnaiah (1999)

As pipe moves upward, the void left by the pipe movement is filled by soil following. At moderate to large displacement, large plastic strains accumulate and form several no of below ground zone shear bands. Details of

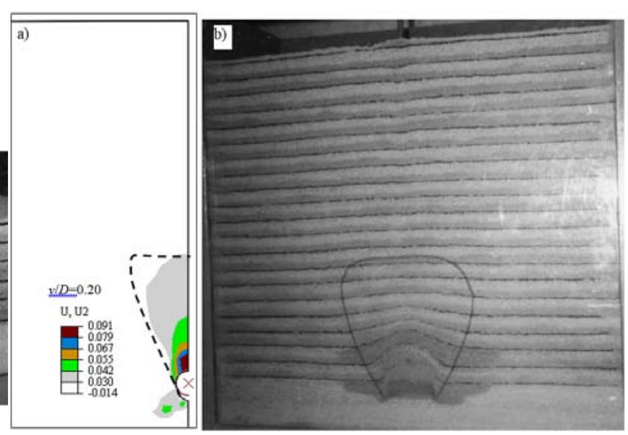

Figure 12. Soil failure mechanism for deep burial condition (Uplift): (a) Present FE analysis results (b) Test results for anchor, Ilamparuthi and Muthukrishnaiah (1999)

the failure pattern developed with MMC model can be found at authors' previous studies, Roy et al. (2015).

6 CONCLUSIONS

The pipeline–soil interactions associated with relative movement of the pipeline in the lateral and upward directions are numerically investigated in this study. The FE simulations are performed in two-dimensional plane strain condition. The key features considered in modeling of the behavior of dense sands are: (i) the decrease of peak friction angle with increase in mean effective stress, (ii) an improved stress–strain behavior of dense sand, including the pre-peak hardening and post-peak softening with plastic shear strain; and (iii) plane strain strength parameters. The FE modeling is performed using Abaqus/Explicit FE software. The FE results with the MMC model are compared with some of the available experimental test results and also with available design charts. Results show the peak dimensionless force vs *H*/*D* curves are consistent with the available design charts for shallow burial condition. However, at deep burial condition, present FE results with the MMC model predict lower peak forces than design guidelines and FE results with MC model. The trend of present FE analysis is similar to the trend of some experimental tests although very limited number of tests are available for deep burial condition. A simplified failure wedge proposed in previous studies is reasonable for shallow burial depth. However, for deep burial condition, a clear wedge does form, but behind the pipe, the plastic shear strains develop in a relatively large zone and sand moves into the gap created by pipe displacements. Further studies are required for proper understanding of failure mechanism at deep burial condition.

ACKNOWLEDGEMENTS

The work presented in this paper was funded by the Research and Development Corporation (RDC), Newfoundland and Labrador and NSERC Discovery and CRD grants.

REFERENCES

American Lifelines Alliance. 2001. Seismic design guidelines for water pipelines. American Lifelines Alliance in partnership with the Federal Emergency Management Agency, Washington, D.C. Available from www.americanlifelinesalliance.org [accessed 4 April 2015].

Audibert, J.M.E., and Nyman, K.J. 1978. Soil restraint against horizontal motion of pipes. International Journal of Rock Mechanics and Mining Sciences and Geomechanics Abstracts, 15(2): A29−A29.

Bolton, M. D. 1986. The strength and dilatancy of sands. Geotechnique, 36(1):65−78.

Byrne, B. W., Schupp, J., Martin, C. M., Oliphant, J., Maconochie, A. and Cathie, D. 2008. Experimental modeling of the unburial behaviour of pipelines. Proc. Offshore Technol. Conf., Houston, TX, paper OTC-2008-19573.

Cheuk, C. Y., White, D. J. and Bolton, M. D. 2008. Uplift mechanisms of pipes buried in sand. Journal of Geotechnical and Geoenvironmental Engineering, 134(2):154–163.

Chin, E. L., Craig, W. H., and Cruickshank, M. 2006. Uplift resistance of pipelines buried in cohesionless soil. Proc., 6th Int. Conf. on Physical Modelling in Geotechnics. Ng, Zhang, and Wang, eds., Vol.1, Taylor & Francis Group, London, pp. 723–728.

Daiyan, N., Kenny, S., Phillips, R., and Popescu, R. 2011. Investigating pipeline–soil interaction under axial–lateral relative movements in sand. Canadian Geotechnical Journal, 48(11):1683−1695.

Dickin, E.A., and Leung, C.F. 1983. Centrifugal model tests on vertical anchor plates. Journal of Geotechnical Engineering, 109(12):1503−1525.

DNV 2007 (Det Norske Veritas). DNV-OS-F101. Available from https://exchange.dnv.com/servicedocuments/dnv/ [accessed 4 April 2015].

Guo, P., and Stolle, D. 2005. Lateral pipe-soil interaction in sand with reference to scale effect. Journal of Geotechnical and Geoenvironmental Engineering, 131(3):338−349.

Honegger, D., and Nyman, D.J. 2004. Guidelines for the seismic design and assessment of natural gas and liquid hydrocarbon pipelines. Pipeline Research Council International, Catalog No. L51927, October.

Ilamparuthi, K. and K. Muthukrishnaiah. 1999. Anchors in sand bed: Delineation of rupture surface. Ocean Eng., 26: 1249-1273.

Jung, J., O'Rourke, T., and Olson, N. 2013. Lateral soil-pipe interaction in dry and partially saturated sand. Journal of Geotechnical and Geoenvironmental Engineering, 139(12): 2028−2036.

Jung, J., O'Rourke, T., and Olson, N. 2013. Uplift soil–pipe interaction in granular soil. Canadian Geotechnical Journal, 50(7):744−753. doi: 10.1139/cgj-2012-0357.

Kouretzis, G.P., Sheng, D., and Sloan, S.W. 2013. Sand-pipeline-trench lateral interaction effects for shallow buried pipelines. Computers and Geotechnics, 54:53-59.

Loukidis, D. and Salgado, R. 2010. Effect of relative density and stress level on the bearing capacity of footings on sand. Géotechnique, 61(2):107–119.

O'Rourke, and M.J., Liu, X. 2012. Seismic design of buried and offshore pipelines. MCEER Monograph, MCEER-12-MN04.

Paulin, M. J. 1998. An investigation into pipelines subjected to lateral soil loading. PhD thesis, Memorial University of Newfoundland, St. John's, Canada.

Roy. Kshama.S., Hawlader B.C., Kenny, S. and Moore, I. 2015. Effect of post-peak softening behavior of dense sand on lateral and upward displacement of buried pipelines. 34th International Conference on Ocean, Offshore and Arctic Engineering (OMAE2015), St. John's, Newfoundland and Labrador, Canada, May 31-June 5, 2015.

Roy. Kshama.S., Hawlader B.C. and Kenny, S. 2014. Influence of Low Confining Pressure on Lateral Soil/Pipeline Interaction in Dense Sand. 33rd International Conference on Ocean, Offshore and Arctic Engineering (OMAE2014), San Francisco, California, USA, June 8-13, 2014.

Roy. Kshama.S., Hawlader B.C., Kenny, S. and Moore, I. 2014. Finite Element Modeling of Uplift Pipeline/Soil Interaction in Dense Sand. Geohazards6, Kingston, Ontario, Canada, June 15-18, 2014.

Schupp, J., Byrne, B. W., Eacott, N., Martin, C. M., Oliphant, J., Maconochie, A., and Cathie, D. 2006. Pipeline unburial behaviour in loose sand. Proc., 25th Int. Conf. on Offshore Mechanics and Arctic Engineering, Hamburg, Germany, OMAE2006-92541.

Trautmann, C. 1983. Behavior of pipe in dry sand under lateral and uplift loading. PhD thesis, Cornell University, Ithaca, NY.

Trautmann, C.H. and O'Rourke, T.D. 1985. Uplift force− displacement response of buried pipe. Journal of Geotechnical Engineering, ASCE, 111(9):1061−1076.

Trautmann, C.H. and O'Rourke, T.D. 1983. Load-Displacement characteristics of a buried pipe affected by permanent earthquake ground movements. Earthquake Behavior and Safety of Oil and Gas Storage Facilities, Buried Pipelines and Equipment, PVP-77, ASME, New York, June, pp. 254-262.

Wang, J., Ahmed, R., Haigh, S. K., Thusyanthan, N. I. and Mesmar, S. 2010. Uplift resistance of buried pipelines at low cover diameter ratios. Proc. Offshore Technol. Conf., Houston, TX, paper OTC-2010-20912.

White, D. J., Barefoot, A. J., and Bolton, M. D. 2001. Centrifuge modeling of upheaval buckling in sand. Int. J. Physical Modeling in Geotechnics, 2(1):19–28.

White, D. J., Cheuk, C. Y., and Bolton, M. D. 2008. The uplift resistance of pipes and plate anchors buried in sand. Geotechnique, 58(10), 771–777.

Wijewickreme, D., Karimian, H., and Honegger, D. 2009. Response of buried steel pipelines subjected to relative axial soil movement. Canadian Geotechnical Journal, 46(7):735−735.

Williams, E.S., Byrne, B.W. and Blakeborough, A. 2013. Pipe uplift in saturated sand: rate and density effects. Geotechnique, 63(11): 946–956.

Xie, X. 2008. Numerical analysis and evaluation of buried pipeline response to earthquake-induced ground fault rupture. PhD thesis, Rensselaer Polytechnic Institute, New York.

Yimsiri, S., Soga, K., Yoshizaki, K., Dasari, G., and O'Rourke, T. 2004. Lateral and upward soil-pipeline interactions in sand for deep embedment conditions. Journal of Geotechnical and Geoenvironmental Engineering, 130(8):830−842.